

## Electron vortices in the amplitude of the atomic ionization by a few-cycle circularly polarized laser pulse

M. A. H. B. Md Yusoff<sup>1</sup>, J. M. Ngoko Djiokap<sup>1</sup>, A. V. Meremianin<sup>2</sup>, and N. L. Manakov<sup>2</sup>

<sup>1</sup>*Department of Physics and Astronomy, University of Nebraska, Lincoln, Lincoln, Nebraska 68588-0299, USA*

<sup>2</sup>*Department of Physics, Voronezh State University, Voronezh 394018, Russia*



(Received 24 May 2024; accepted 16 July 2024; published 2 August 2024)

Electron vortices emerging in the amplitude of the ionization of an atom by an isolated few-cycle, circularly polarized electromagnetic pulse are analyzed in the multiphoton regime. We demonstrate that the number of vortices, as well as their position and strength, are determined by the relative magnitudes of the dynamical amplitude parameters corresponding to sequential photon absorption. It is shown that the phase maps of the ionization amplitude in the momentum space exhibit spiral structures, which are signatures of the Coulomb scattering phases.

DOI: [10.1103/PhysRevA.110.023102](https://doi.org/10.1103/PhysRevA.110.023102)

### I. INTRODUCTION

Recently, the question of the interaction of beams carrying orbital angular momentum with atoms has attracted much attention [1–10]. Such beams (often called twisted or vortex beams) bear well-defined values of the integer orbital momentum quantum number  $m$ , which describes the dependence of the corresponding wave function on the azimuthal angle  $\varphi$  through the factor  $\exp(im\varphi)$  (for beams propagating along the  $z$  axis). For the points on the  $z$  axis the angle  $\varphi$  is undefined, and therefore the wave function there has to be zero. Accordingly, the velocity field,  $\mathbf{v}(\mathbf{r}) = \text{Im}(\psi^* \nabla \psi) / |\psi|^2$ , is swirling around the propagation direction of the twisted beam. This swirl, or vortex, is characterized by the parameter  $M$ , defined by

$$M = \frac{1}{2\pi} \oint_K \mathbf{v}(\mathbf{r}) \cdot d\mathbf{r} = \frac{1}{2\pi} \oint_K \frac{\text{Im}(\psi^* \nabla \psi)}{|\psi|^2} d\mathbf{r}, \quad (1)$$

where  $K$  denotes an (arbitrary) contour encircling the  $z$  axis.

The theoretical background of the above property of the twisted (or vortex) beams is based on the pioneering work by Dirac [11], who noted that when the wave function,  $\psi$ , of a quantum particle is zero in every point on a line (the nodal line, which is not necessarily a straight line), the circulation of the velocity field around that line is a quantized quantity, see Eq. (1). In Eq. (1)  $M$  can take only integer values,  $M = 0, \pm 1, \pm 2, \dots$ . When depicted, the velocity field in the vicinity of a nodal line has the form of a swirl, which is why such phenomena are referred to as “quantum vortices” [1, 12–14]. The parameter  $M$  is called “vorticity number,” “vortex strength,” or the “topological charge” of a vortex. Since a nodal point is defined by two conditions,  $\text{Re} \psi = 0$  and  $\text{Im} \psi = 0$ , we conclude that the points in space where  $\psi = 0$  can be lines (nodal lines) or surfaces (nodal surfaces). In the latter case the vorticity number of every point of the nodal surface is equal to zero (otherwise it would be infinite, since any two points on a nodal surface can be connected by infinitely many nodal lines). Below we will denote quantum

states for which the velocity field has vortices as “vortex states.” General properties of such states were analyzed in [15–17].

For the sake of illustration of these two types of nodal structures, let us consider bound states of the quantum particle in a Coulomb field. In this case the wave function can be written in the form [18]

$$\psi(\mathbf{r}) = R_{nl}(r)Y_{lm}(\hat{\mathbf{r}}) = R_{nl}(r)Y_{lm}(\theta, 0) e^{im\varphi}, \quad (2)$$

where  $r, \theta, \varphi$  are spherical coordinates of the radius vector  $\mathbf{r}$ ;  $R_{nl}(r)$  is the radial part of the wave function with the principal quantum number  $n$ ; and  $Y_{lm}(\theta, \varphi)$  is the spherical harmonic with the orbital momentum  $l$  and the magnetic quantum number  $m$ . For the ground state,  $l = m = 0, n = 1$  and the radial part of  $\psi$  has no nodes. For the excited states, there are several possibilities. For  $S$  states, one has  $l = m = 0$  and  $\psi$  is a real-valued function, which has zeros for some values of  $r$ . Thus, zeros of  $S$  states form concentric spheres in space, which are the nodal surfaces. Each point on such spheres is a zero-strength vortex,  $M = 0$ . For  $P$  states,  $l = 1$  and  $m = 0, \pm 1$ , zeros of the radial functions  $R_{n1}(r)$  ( $n > 2$ ),  $R_{n1}(r_0) = 0$ , form nodal surfaces as the series of concentric spheres. Moreover, the angular part of a  $P$  state for  $m = 0$  is zero at  $\theta = \pi/2$ , which defines the  $xy$  plane as a nodal surface, while for  $m = \pm 1$ , one has  $\theta = 0, \pi$ , which defines the  $z$  axis as a nodal line. Thus, vortices in the wave functions of  $P$  states with  $m = \pm 1$  occur on the points of the  $z$  axis. In this case it is convenient to choose the contour  $K$  to be a circle in the  $xy$  plane. Consequently, the integral in Eq. (1) evaluates to

$$\begin{aligned} M &= \frac{1}{2\pi} \oint_0^{2\pi} \frac{\text{Im}(\psi^* \partial \psi / \partial \varphi)}{|\psi|^2} d\varphi \\ &= \frac{m}{2\pi} \oint_0^{2\pi} d\varphi = m. \end{aligned} \quad (3)$$

As is seen, a  $P$  state has one vortex whose strength is equal to the value of the magnetic quantum number  $m$ . For states with higher-order orbital momentum, the situation is similar.

Vortices only emerge on the  $z$  axis when the magnetic quantum number  $m \neq 0$ , and their strength is equal to  $m$ . One can show [11,19] that an additional phase, acquired by the wave function circulating along a contour enclosing a nodal line, is connected to a magnetic flux through that contour. Thus, the quantization of the velocity field circulation implies the quantization of a magnetic flux. In our example that magnetic flux is generated by the (quantized) orbital motion of the electron. It is interesting that the scattering wave function of the Coulomb problem has no nodes [18]. We note that the nodal structure of the wave functions of the helium atom was analyzed in several works; see, e.g., Refs. [20–23]. However, the occurrence of quantum vortices in the helium atom was not investigated by the respective authors.

It is important that quantum vortices may occur not only in the wave functions but also in the amplitudes of various fragmentation processes, such as impact ionization [24–27]. The corresponding amplitude is a complex-valued function of the momentum of an escaping electron, and quantum vortices could emerge in the momentum space. In the conventional photoionization process induced by a monochromatic electromagnetic pulse having the frequency  $\omega$ , the energy of the photoelectron is fixed by the equation  $E = p^2/2 = E_i + \hbar\omega$  ( $E_i < 0$  is the energy of the initial bound state), and the photoelectron momentum distribution (PMD) is a sphere in momentum space. During the last decades it became possible to observe the ionization of atoms by the ultrashort (few-cycle) laser pulses [28–33]. Few-cycle pulses are broadband, and therefore the energy (and momentum) of the photoelectron can vary in a certain range. Thus, the PMD occupies a certain volume in momentum space. Accordingly, the amplitude of the short-pulse ionization process,  $A$ , is a function of the magnitude  $p$  of the momentum vector and its direction  $\hat{\mathbf{p}} = \mathbf{p}/p$ . The connection between nodal structures and quantum vortices in the wave function discussed in the paragraph above raises the overarching question as to where and how quantum vortices occur in the ionization amplitude  $A(\mathbf{p})$ .

The simplest way to answer this question is to analyze the situation when the ionization is performed by purely circularly polarized (CP) pulses. The structure of quantum vortices in the amplitude of the photodetachment by CP pulses was analyzed in the series of works [34–37] where the process was considered both in the multiphoton and strong-field regimes. Formation of electron vortices in strong-field ionization was the subject of recent works [5,38,39]. In this article we investigate the occurrence of quantum vortices in the ionization amplitudes of atoms by a single intense, few-cycle CP pulse in the multiphoton regime.

Before considering the case of a single CP pulse, it is important to highlight that interesting phenomena occur when an atom (or a molecule) is ionized by a pair of time-delayed CP pulses with moderate intensities. It was shown [40–44] that for corotating CP pulses, the PMDs for the threshold electron exhibit interference fringes in the form of concentric circles, similar to Newton’s interference rings; meanwhile, for counter-rotating CP pulses, the interference is seen in the form of Fermat spirals. It is remarkable that the number of arms in those spirals is determined by the number of absorbed photons [45]. (This rule may be violated for counter-rotating elliptically polarized pulses [46].) Although spiral structures

in the PMDs were termed “vortices” [40–42,45,47], they are not the same as quantum vortices in the above sense, which are defined as nodal lines with nonzero circulation of the velocity field. These velocity field vortices are not seen in PMDs as any kind of spiral structures. Rather, they can be identified in the phase maps of the ionization amplitude, where they occur in the form of finger- or forklike patterns [48].

The goal of the present work is to analyze properties of quantum vortices in the amplitude of the ionization of atoms by a single intense, few-cycle CP pulse. Namely, we investigate where in momentum space such vortices occur and what is their strength. Besides the quantum vortex occurring at the origin in momentum space, we will show that the interference of ionization amplitudes corresponding to the sequential orders of the photon absorption (e.g., one- and two-photon, etc.) causes the emergence of additional amplitude quantum vortices. Interestingly, the same interference effect that causes the occurrence of quantum vortices in the ionization amplitude also underlies the occurrence of the circular dichroism in the ionization of atoms by an intense few-cycle pulse [49,50]. Although we assume the ionization to be performed in the perturbative regime, our conclusions may well be valid for stronger pulse intensities, since in this case similar “dynamic” interference effects take place [51–53]. It is remarkable that although ionization amplitude vortices do not appear as spirals in the corresponding momentum distribution, some spiral patterns are inherent to the process of the short CP pulse ionization. Namely, we found that the phase maps of the ionization amplitude exhibit spiral patterns. The number of arms of those spirals is equal to the number of absorbed photons. We emphasize that such spirals do not occur in the photodetachment process [19,35]. It will be shown below that the spiral patterns in the phase maps of the ionization amplitude are signatures of the Coulomb scattering phases,  $\delta_l(p)$ . Therefore, we denote these patterns as “Coulomb spirals.”

The paper is organized as follows. In Sec. II we derive the parametrization of the amplitude of the ionization by a single intense, few-cycle CP pulse. We consider the situation when the pulse parameters lie within the range where the nonstationary perturbation theory (PT) is applicable. We obtain conditions which lead to the occurrence of quantum vortices in the ionization amplitude. Results of our PT analysis are compared with the results of numerical solution of time-dependent Schrödinger equation (TDSE) for hydrogen and helium atoms in Sec. III. Some concluding remarks are given in Sec. IV, together with an outlook for further research. In Appendix we calculate the integral defining the circulation of the ionization amplitude velocity field.

Atomic units are used throughout the text unless otherwise specified.

## II. PERTURBATION THEORY ANALYSIS OF VORTICES IN THE PHOTOIONIZATION AMPLITUDE

First, in Sec. II A we derive the PT parametrization of the ionization amplitude. Next, in Sec. II B properties of vortices occurring in the ionization amplitude are analyzed. Finally, in Sec. II C we discuss the origin of spiral patterns emerging in the phase maps of the ionization amplitude.

### A. Parameterization of the ionization amplitude

We will analyze the ionization amplitude,  $\mathcal{A}$ , corresponding to the emission of an electron by an atom subjected to a few-cycle CP electromagnetic pulse. We define the electric field strength vector by

$$\mathbf{F}(t) = \text{Re} [\mathbf{e} F(t) e^{-i(\omega t + \phi)}]. \quad (4)$$

Here  $\omega$  is the pulse carrier frequency,  $F(t)$  is the pulse envelope function,  $\phi$  is the carrier envelope phase (CEP), and  $\mathbf{e}$  is the complex vector of the pulse polarization. For the sake of simplicity, below we do not consider CEP effects and we set  $\phi = 0$ . For CP pulses the polarization vector can be written in the following form [49],

$$\mathbf{e} = \frac{1}{\sqrt{2}} (\mathbf{e}_x + i\xi \mathbf{e}_y), \quad \xi = \pm 1, \quad (5)$$

where  $\mathbf{e}_x, \mathbf{e}_y$  are unit vectors of the Cartesian basis, with its  $z$  axis directed along the pulse propagation. Throughout this work, we define left and right from the point of view of the emitter of the laser source, as commonly used in the synchrotron radiation community. For right-hand CP (RCP) one has  $\xi = 1$ , while  $\xi = -1$  for left-hand CP (LCP) pulses. The polarization vector is normalized by the condition  $(\mathbf{e}^* \cdot \mathbf{e}) = 1$ . The linear polarization degree for purely CP pulses is equal to zero,  $\ell = (\mathbf{e} \cdot \mathbf{e}) = 0$ .

Within the time-dependent perturbation theory, the amplitude of the ionization by a broadband (i.e., few-cycle) electromagnetic pulse can be presented as a sum of terms, corresponding to different PT orders. In [54,55] it was shown that the dependence of the ionization amplitude on the photoelectron emission angles for the ionization of an initial state with the angular momentum quantum numbers  $l_i m_i$ , which is caused by an absorption of  $n$  CP photons with the frequency  $\omega$ , can be parameterized as follows:

$$A_n = \sum_{l=|l_i-n|}^{l_i+n} R_l(p) \{Y_l(\hat{\mathbf{p}}) \otimes \{\mathbf{e}\}_n\}_{l_i m_i}, \quad (6)$$

where  $R_l(p)$  are radial partial amplitudes,  $\hat{\mathbf{p}}$  is the unit vector along the photoelectron momentum  $\hat{\mathbf{p}} = \mathbf{p}/p$ ,  $\{Y_l(\hat{\mathbf{p}}) \otimes \{\mathbf{e}\}_n\}_{l_i m_i}$  are irreducible tensor products [56] of spherical harmonics  $Y_{lm}(\hat{\mathbf{p}})$ , depending on the angles of  $\hat{\mathbf{p}}$ , with the minimal tensor product of  $n$  polarization vectors  $\mathbf{e}$ ,  $\{\mathbf{e}\}_{nm_n}$ , defined by [54]

$$\{\mathbf{e}\}_{nm_n} = \{\{\dots\{\{\mathbf{e} \otimes \mathbf{e}\}_2 \otimes \mathbf{e}\}_3 \dots \mathbf{e}\}_{n-1} \otimes \mathbf{e}\}_{nm_n}. \quad (7)$$

Note that the tensor product (7) does not depend on the coupling scheme of vectors  $\mathbf{e}$ . For CP photons the spherical components of  $\mathbf{e}$  have the form [cf. Eq. (5)]

$$\begin{aligned} e_0 &= (\mathbf{e} \cdot \mathbf{e}_z) = 0, \\ e_{\pm 1} &= \mp \frac{1}{\sqrt{2}} [(\mathbf{e} \cdot \mathbf{e}_x) \pm i(\mathbf{e} \cdot \mathbf{e}_y)] = \frac{\xi \mp 1}{2}. \end{aligned} \quad (8)$$

Here, the last equation can be rewritten as

$$e_\mu = \xi \delta_{\mu, -\xi}, \quad \mu = \pm 1. \quad (9)$$

As a consequence, we have that the only nonzero component of the tensor product (7) of vectors  $\mathbf{e}$ , defined by Eq. (5), is

that with  $m_n = -\xi n$ :

$$\{\mathbf{e}\}_{nm_n} = \delta_{m_n, -\xi n} \xi^n. \quad (10)$$

Below we limit our consideration only to the case of the electronic emission in the pulse polarization plane, which is the  $xy$  plane, corresponding to the polar spherical angle  $\theta = \pi/2$ . In this case the spherical harmonics in Eq. (6) can be written explicitly as follows [56]:

$$\begin{aligned} Y_{lm} \left( \frac{\pi}{2}, \varphi \right) \\ = (-1)^{\frac{l+m}{2}} e^{im\varphi} \sqrt{\frac{2l+1}{4\pi} \frac{(l+m-1)!! (l-m-1)!!}{(l+m)! (l-m)!}}, \end{aligned} \quad (11)$$

where  $l+m$  is an even number, otherwise  $Y_{lm}(\pi/2, \varphi) = 0$ . In Eq. (11)  $\varphi$  is the polar angle of the momentum vector  $\mathbf{p}$  in the  $xy$  plane, where the pulse electric field vector  $\mathbf{E}$  is rotating.

Equations (10) and (11), together with the properties of the Clebsch-Gordan coefficients entering the tensor product (6), allow one to present the amplitude of the  $n$ -photon ionization in the following form:

$$A_n = e^{i(m_i + \xi n)\varphi} \mathcal{A}_n(p), \quad (12)$$

where  $\mathcal{A}_n(p)$  is the dynamical parameter, depending on the energy of the photoelectron but not on its emission direction. As was noted above, the total ionization amplitude is a sum of terms corresponding to different numbers of absorbed photons:

$$A(\mathbf{p}) = \sum_{n=1}^{\infty} e^{i(m_i + \xi n)\varphi} \mathcal{A}_n(p) = e^{im_i\varphi} \sum_{n=1}^{\infty} e^{i\xi n\varphi} \mathcal{A}_n(p). \quad (13)$$

### B. Vortices in the ionization amplitude

Let us consider the question on the positions of the zeros of the ionization amplitude  $A(\mathbf{p})$  in the  $xy$  plane. Let  $\mathbf{p}_0 = (p_0, \varphi_0)$  be the polar coordinates of the momentum vector corresponding to the zero of the amplitude, that is,  $A(\mathbf{p}_0) = 0$ . This zero (i.e., the node) is characterized by the topological charge (or the vortex number)  $M(p_0)$ , defined by [cf. Eq. (1)]

$$M(p_0) = \frac{1}{2\pi} \oint_K \frac{\text{Im}(A^* \nabla A)}{|A|^2} d\mathbf{p} = \frac{1}{2\pi} \oint_K \text{Im} \nabla(\ln A) d\mathbf{p}, \quad (14)$$

where  $\nabla = \partial/\partial\mathbf{p}$ , and the integration contour  $K$  encloses the point  $\mathbf{p} = \mathbf{p}_0$  in the  $xy$  plane. In this case  $p_z = 0$ , and therefore  $\nabla$  is a two-dimensional gradient operator whose Cartesian components are  $\nabla = (\partial/\partial p_x, \partial/\partial p_y)$ . Let us evaluate the circulation of the logarithmic derivative of the ionization amplitude  $A(\mathbf{p})$ :

$$\Gamma(A) = \oint_K \nabla g(\mathbf{p}) \cdot d\mathbf{p}, \quad g(\mathbf{p}) = \ln A(\mathbf{p}). \quad (15)$$

The polar coordinates of the momentum vector  $\mathbf{p}$  are  $p$  and  $\varphi$ , and Cartesian coordinates of  $\mathbf{p}$  are

$$\mathbf{p} = p(\cos \varphi, \sin \varphi). \quad (16)$$

The vector element of the contour can be written as

$$d\mathbf{p} = \hat{\mathbf{p}} dp + p\boldsymbol{\tau} d\varphi, \quad (17)$$

where the unit vector  $\boldsymbol{\tau} = (-\sin\varphi, \cos\varphi)$  is perpendicular to  $\hat{\mathbf{p}} = \mathbf{p}/p$ . The gradient operator written in cylindrical coordinates has the form

$$\nabla = \hat{\mathbf{p}} \frac{\partial}{\partial p} + \frac{\boldsymbol{\tau}}{p} \frac{\partial}{\partial \varphi}. \quad (18)$$

Inserting Eq. (18) into Eq. (15) for the circulation, we obtain,

$$\Gamma(A) = \oint_K \frac{1}{A(\mathbf{p})} \left( \frac{\partial A(\mathbf{p})}{\partial p} dp + \frac{\partial A(\mathbf{p})}{\partial \varphi} d\varphi \right). \quad (19)$$

If the amplitude can be written in a factorized form, then from Eq. (14) we have that the topological charge inside some contour is a sum of charges corresponding to different amplitude factors. From Eq. (13) it is seen that the factor  $\exp(im_i\varphi)$  is common for all PT orders. Now let  $K$  be a small circle with its center at  $p = 0$ . Then, from Eq. (14) we obtain that the topological charge in the point  $p = 0$  is equal to the magnetic quantum number of the initial bound state, i.e.,  $M(0) = m_i$ . If the common factor of the amplitude is a function of  $p$ , which has no nodes in the  $xy$  plane, then, according to Eq. (14), it can be ignored when calculating the topological charge.

It is convenient to write the dynamical ionization amplitude parameters (13) as follows:

$$A_n(p) = A_n(p) e^{i\alpha_n(p)}, \quad n = 1, 2, \dots, \quad (20)$$

where the absolute values  $A_n(p)$ , and arguments  $\alpha_n(p)$ , are functions of the momentum  $p$  (or the energy  $E = p^2/2$ ) and are independent of the angle  $\varphi$ . For a monochromatic pulse the dynamical parameters are proportional to Dirac  $\delta$  functions,  $A_n(p) \sim \delta(p^2/2 - n\omega - I_p)$ , where  $I_p = |E_i|$  is the ionization potential, which is the consequence of the energy conservation law. For a broadband pulse in the PT regime the absolute value  $A_n(p)$  has maximum in the vicinity of the point  $p_n = \sqrt{2(n\omega - I_p)}$  and decreases to zero as  $p$  deviates further from  $p_n$ . Hence, the non-negative functions  $A_n(p)$  are intersecting for some values of momenta located between their maxima separated by the energy  $\approx \hbar\omega$ . This means that the photoelectron with the energy  $E \approx n\omega - I_p$  could be emitted due to the absorption of either  $n$  or  $n \pm 1$  photons. The coexistence of competing ionization channels is caused by the fact that the energy of the photons in a few-cycle pulse is not a well-defined quantity. Rather, it lies within some range around the energy  $\hbar\omega$ , corresponding to the carrier frequency. The shorter the pulse, the broader the photon energy range. Thus, for the photoelectron energy satisfying the condition  $n\omega \leq E + I_p \leq (n+1)\omega$ , the main contribution into the expansion (13) of the ionization amplitude comes from three terms,

$$A(\mathbf{p}) = e^{i(m_i + \xi n)\varphi} \left( A_{n-1} e^{i(\alpha_{n-1} - \xi\varphi)} + A_n e^{i\alpha_n} + A_{n+1} e^{i(\alpha_{n+1} + \xi\varphi)} \right). \quad (21)$$

Numerical TDSE results obtained for the ionization of hydrogen and helium atoms (see Sec. III) demonstrate that in the PT regime the main contribution into the ionization amplitude in the vicinity of a vortex comes from only two terms:

$$A(\mathbf{p}) = e^{i(\alpha_n + (m_i + n\xi)\varphi)} \left( A_n + A_{n+1} e^{i(\xi\varphi + \beta)} \right), \quad (22)$$

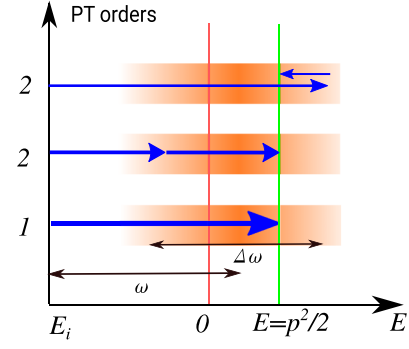


FIG. 1. The mechanism of the multiphoton ionization by a few-cycle pulse within PT.  $E_i < 0$  is the energy of the initial bound state,  $E = p^2/2$  is the photoelectron energy, and  $\omega$  and  $\Delta\omega$  are pulse carrier frequency and its bandwidth. The thicker the line, the larger the process probability.

where  $\beta = \alpha_{n+1} - \alpha_n$ , and  $n$  is the largest integer less than  $I_p/\hbar\omega$ . If  $\hbar\omega \approx I_p$ , then  $A_1$  and  $A_2$  are the first- and the second-order PT amplitudes, respectively. The amplitude in the first PT order can be interpreted as a single-photon absorption process. In the second PT order there are two possible processes [49], see Fig. 1: (i) two-photon absorption and (ii) one-photon absorption + one-photon emission. For the two-photon absorption process, the dependence of the amplitude on the angle  $\varphi$  is defined by the function  $\exp(2i\xi\varphi)$ ; meanwhile, for the process of one-photon absorption + one-photon emission, the dependence on  $\varphi$  cancels out. Numerical TDSE results (see Sec. III below) demonstrate that in the PT regime the contribution of the channel (ii) is negligibly small. This means that the ionization amplitude in this case can indeed be presented as a combination of only two terms [see Eq. (22)]:

$$A(\mathbf{p}) = e^{i[\alpha_1 + (m_i + \xi)\varphi]} \left( A_1 + A_2 e^{i(\xi\varphi + \beta)} \right), \quad (23)$$

where  $\beta = \alpha_2 - \alpha_1$ .

It is clear that zeros of the amplitudes in Eqs. (22) and (23) occur in points where the functions  $A_n(p)$ ,  $A_{n+1}(p)$  are equal and the angle  $\varphi$  is

$$\varphi = \varphi_0 = \pi + \xi (\alpha_n - \alpha_{n+1}). \quad (24)$$

In order to calculate the corresponding topological charge, it is convenient to choose the contour  $K$ , enclosing the zero of the ionization amplitude, to be composed of two radial and two arc segments, see Fig. 7. Details of the calculation of the circulation in Eq. (14) are given in Appendix, where it is shown that the topological charge of the vortex in the ionization amplitude having the form (22) is equal to  $\pm 1$ , depending on the type of the crossing of curves  $A = A_n(p)$  and  $A = A_{n+1}(p)$ . If the curves intersect as shown in Fig. 2(a), then the topological charge equals  $\xi$ ; if the intersection occurs in the point where the function  $A_{n+1}(p)$  decreases, point 2 in Fig. 2(b), then the topological charge is  $-\xi$ . Apart from that, the ionization amplitude vortices can have charges with absolute values larger than 1 when three or more terms give comparable contribution into the amplitude, as in Eq. (21). Namely, zeros of the amplitude in the form (21) are defined by solutions of the quadratic equation

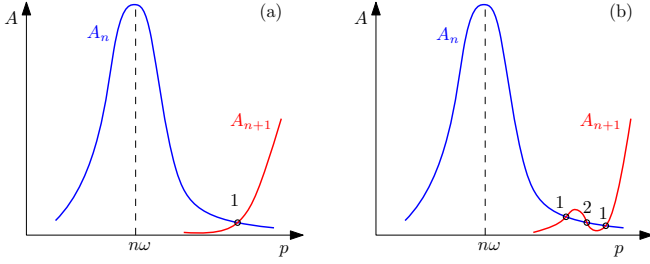


FIG. 2. Possible crossings of the curves of dynamical ionization amplitude parameters  $A_n$  and  $A_{n+1}$ , corresponding to the absorption of  $n$  and  $n + 1$  photons. The crossing in (a) leads to a single vortex with the topological charge  $\xi$ ; the crossings (b) lead to three vortices with the same total charge  $\xi$ . Vortices in 1 have the charge  $\xi$ , in 2 the charge is equal to  $-\xi$ .

[below  $z = \exp(i\xi\varphi)$ ]:

$$\begin{aligned} z^2 + bz + c &= 0, \\ b &= \frac{A_n}{A_{n+1}} e^{i(\alpha_n - \alpha_{n+1})}, \\ c &= \frac{A_{n-1}}{A_{n+1}} e^{i(\alpha_{n-1} - \alpha_{n+1})}, \end{aligned} \quad (25)$$

which satisfy the condition  $|z| = 1$ . It is obvious that Eq. (25) has no more than two solutions, which coincide when the condition  $b = 2c^{1/2}$  is met. If this happens in some point  $\mathbf{p}_0 = (p_0, \varphi_0)$ , then we have that  $A_{n+1}(p_0) = A_{n-1}(p_0) = A_n(p_0)/2$  and  $\alpha_n(p_0) = [\alpha_{n+1}(p_0) + \alpha_{n-1}(p_0)]/2 + 2\pi k$ ,  $k = 0, \pm 1, \pm 2, \dots$ . After these conditions are met, it could be possible that the ionization amplitude in the vicinity of  $\mathbf{p}_0$  can be written as

$$A(\mathbf{p}) = A_{n+1}(p) e^{i[(n-1)\xi\varphi + i\alpha_{n+1}]} (e^{i\xi\varphi} + e^{i\Delta\alpha/2})^2, \quad (26)$$

where  $\Delta\alpha = \alpha_{n-1} - \alpha_{n+1}$ . Since Eq. (14) contains the logarithmic derivative, we obtain that the topological charge in  $\mathbf{p}_0$  is equal to twice the topological charge of the function  $(\exp i\xi\varphi + \exp i\Delta\alpha/2)$ , which is equal to  $\pm\xi$ , as was noted above. We note that for all pulse parameters considered in our TDSE examples (see Sec. III), we have never encountered situations where the change in topological charges was not equal to 1.

Let us consider the situation when the photoelectron energy is close to  $n\omega - I_p$ . As was explained above, in this case the ionization amplitude can be presented as a combination of three terms, see Eq. (21). If we choose the integration contour to be the circle with the radius  $p = \sqrt{2(n\omega - I_p)}$ , then from Eqs. (14) and (21) we obtain that the total topological charge inside the contour is determined by the amplitude factor  $\exp[i(m_i + n\xi)\varphi]$ . Consequently, the total charge inside the circle is equal to  $m_i + \xi n$ . Similarly, if we expand the contour so that the radius of the circle is  $\sqrt{2[(n+1)\omega - I_p]}$ , then the total topological charge becomes  $m_i + \xi(n+1)$ . Thus, the topological charge is increased by  $\xi$  whenever an additional photon is absorbed.

The above statement, however, is not quite rigorous, since the change of the total topological charge inside the circular integration contour by  $\xi$  could happen when the ionization amplitude contains ‘‘vortex-antivortex’’ pairs. Indeed, a vortex

has charge  $\xi$ , while an antivortex has charge  $-\xi$ , so that the topological charge of the pair is zero. To clarify this issue, let us consider the ionization amplitude for the photoelectron energy within the interval  $[n\omega - I_p, (n+1)\omega - I_p]$ . Next, let us assume, for the sake of simplicity, that the amplitude can be written as a combination of two terms, see Eq. (22). Within the mentioned energy interval the amplitude of the  $n$ -photon ionization  $A_n$  decreases while the amplitude of the  $(n+1)$ -photon ionization  $A_{n+1}$  increases. Then, in some point  $p = p_0$  curves  $A = A_n(p)$  and  $A = A_{n+1}(p)$  will intersect,  $A_n(p_0) = A_{n+1}(p_0)$ . If that intersection has the form shown in Fig. 2(a), then the corresponding topological charge will be equal to  $\xi$ . If the curves  $A_{n+1}(p)$  and  $A_n(p)$  cross in three points, as is shown in Fig. 2(b), then three vortices will occur with the same total charge  $\xi$ . Now if the radius of the integration contour lies somewhere between points 1 and 2 in Fig. 2(b), then the topological charge inside the contour will increase by  $\xi$  without an absorption of an additional photon. If we further expand the contour beyond point 2, then the total topological charge inside the contour will decrease by  $\xi$ . Note that in our TDSE results (see Fig. 5) we did not observe crossings of the kind Fig. 2(b).

### C. Properties of the ionization amplitude phase

Below we analyze the dependence of the phase of the ionization amplitude on the photoelectron momentum. Let us assume the initial bound state has zero total angular momentum,  $l_i = m_i = 0$ , and the pulse carrier frequency to be  $\omega \sim I_p/\hbar$ . In the PT regime the ionization amplitude in this case is determined by terms corresponding to the transition from the bound  $S$  state into the continuum  $P$  state (first PT order), and continuum  $D$  state (second PT order). As a result, the ionization amplitude can be written in the following form [55] [cf. Eq. (22)]:

$$A_{12} \equiv A(\mathbf{p}) = A_1(p) e^{i(\delta_1 + \pi/2 + \varphi)} + A_2(p) e^{i(\delta_2 + 2\varphi)}, \quad (27)$$

where  $\delta_l$  ( $l = 1, 2$ ) are the Coulomb scattering phases [18],  $\delta_l = \arg \Gamma(1 + l - i/p)$ . To understand the role of the interference emerging after taking the modulus of the amplitude (27), we choose  $A_1(p)$  and  $A_2(p)$ , two smooth curves which intersect according to Fig. 2(a). The curves  $A = A_1(p)$  and  $A = A_2(p)$  are shown in Fig. 3(a). In Figs. 3(b) and 3(c), the absolute value and the phase of the ionization amplitude  $A_{12}$  are shown. It is seen that the presence of the single- and two-photon ionization channels leads to a slight circular asymmetry of the ionization probability in the pulse polarization plane [see Fig. 3(b)]. The dependence of the phase of the amplitude on the angle of the photoelectron momentum,  $\arg A(\varphi)$ , has two remarkable peculiarities. First, for small photoelectron energies the phase jumps by  $2\pi$  on a single-arm spiral. This Coulomb spiral is defined by the equation [see Eq. (27)]

$$\delta_1(p) + \varphi = \pm 3\pi/2. \quad (28)$$

Second, in the lower part of Fig. 2(c), one sees the emergence of the second spiral arm on which the phase jumps by  $2\pi$ . The point on the top end of the second spiral arm corresponds to a quantum vortex where the ionization amplitude vanishes,  $A_{12} = 0$ .

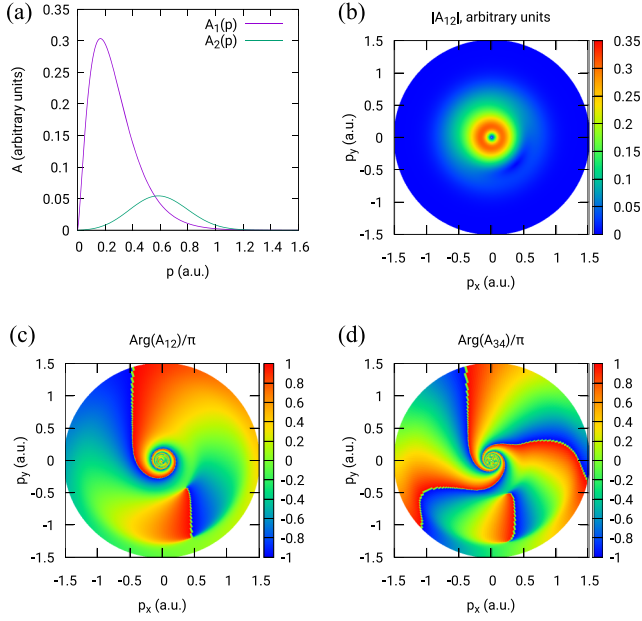


FIG. 3. Momentum distributions for the absolute value (b), and phases (c), (d), of the ionization amplitude, modeled by two consecutive PT amplitude terms, see Eqs. (27) and (29). On the panel (a), the model curves corresponding to the dynamical parameters  $A_1(p)$ ,  $A_2(p)$  are shown.

Now let us assume that the carrier frequency lies in such a range that the ionization event requires the absorption of three photons. According to the PT, in this case the ionization amplitude expresses as a combination of third- and fourth-order PT amplitudes. Let us choose the “radial” functions  $A_n(p)$  for  $n = 3, 4$  to be the same functions  $A_1(p)$ ,  $A_2(p)$ , as in the previous example [see Fig. 3(a)]. Then, the ionization amplitude can be written similarly to Eq. (27), but with different phase factors:

$$A_{34} \equiv \mathbf{A}(\mathbf{p}) = A_1(p) e^{i(\delta_3 - \pi/2 + 3\varphi)} + A_2(p) e^{i(\delta_4 - \pi + 4\varphi)}. \quad (29)$$

The dependence of the phase of the ionization amplitude on the photoelectron momentum and its emission angle is shown in Fig. 3(d). Despite the different dependence of the terms in Eqs. (29) and (27) on the angle  $\varphi$ , the corresponding momentum distribution,  $|A_{34}|$ , is almost identical to  $|A_{12}|$  and therefore is not shown. On the contrary, the phases  $\arg A_{34}$  and  $\arg A_{12}$  are substantially different. In the case of three-photon threshold, the three-arm spiral on which the phase jumps by  $2\pi$  is seen in Fig. 3(d). This three-photon Coulomb spiral is located in the region where the three-photon absorption dominates,  $A_1 \gg A_2$  in Eq. (29), and it is defined by the equation

$$\delta_3(p) + 3\varphi = \pm 3\pi/2. \quad (30)$$

For  $A_1 = A_2$  and the angle  $\varphi$ , which corresponds to the phase difference of terms in (29) being equal to  $\pi$ , there occurs a quantum vortex, which is seen as the formation of the fourth arm of the Coulomb spiral.

The above features of the interference of PT amplitude terms can be summarized as follows: for small values of  $p$ , the momentum distributions of the ionization amplitude phase,

$\arg A(\mathbf{p})$ , exhibit spiral structures with the number of arms equal to the number of absorbed photons; with an increase of the photoelectron energy at some values of the momentum  $p$  and the angle  $\varphi$  the ionization amplitude vanishes ( $A = 0$ ) and there appears a quantum vortex, which is seen as the formation of the additional arm of the phase spiral; further increase of  $p$  eventually leads to the formation of a new vortex and a corresponding additional spiral arm, and so on.

### III. NUMERICAL RESULTS FOR HYDROGEN AND HELIUM ATOMS

Below we compare results of the above-described PT analysis with the results obtained by the numerical solution of the TDSE for the hydrogen and helium atoms. For the H atom we have utilized the numerical package `qprop` [57,58]. The ionization amplitude in `qprop` is defined by the truncated partial expansion,

$$A(\mathbf{p}) = \sum_{l=0}^{l_{\max}} \sum_{m=-l}^l a_{lm}(p) Y_{lm}(\hat{\mathbf{p}}), \quad (31)$$

where  $l_{\max}$  is the maximal value of the photoelectron’s orbital momentum used in the computations. For intensities below  $10^{15} \text{W/cm}^2$  and carrier frequencies  $\omega \geq 0.2$ , the satisfactory convergence is achieved for  $l_{\max} \leq 15$ .

In Fig. 4 we show TDSE results for the absolute value of the amplitude (namely,  $\sqrt{p}|A|$ ) for the ionization of the 1-S ground state of the hydrogen atom by the RCP pulse with the duration of three optical cycles,  $n_c = 3$ , for three values of  $\omega$ : 0.202 a.u. (5.5 eV,  $\lambda = 225.6$  nm), 0.456 a.u. (12.4 eV,  $\lambda = 100$  nm), and 0.513 a.u. (13.95 eV,  $\lambda = 88.8$  nm, ninth harmonic of 800-nm laser [59]). It is seen that in the multiphoton regime (i.e., when PT is valid) the momentum distributions of the ionization amplitude’s absolute value exhibit only slight circular asymmetry. This means that for a given value of  $p$  the main contribution into the total ionization amplitude comes from only one term in the expansion (13). This conclusion is further supported by Fig. 5, where the absolute values of the amplitude parameters  $A_n(p)$  are shown. For  $\omega > 0.2$  a.u., the PMDs exhibit a noticeable asymmetry when the pulse intensity is increased to  $10^{15} \text{W/cm}^2$ , see Fig. 4(b). This means that the total ionization amplitude comprises several terms corresponding to different PT orders, which have comparable magnitude [see Fig. 5(b)]. By comparing results shown in Figs. 4(b), 4(c), and 4(d), we conclude that for a given pulse intensity, the PT works better for larger values of the carrier frequency, which is a known fact [60].

The momentum distributions of the phase of the ionization amplitude are shown in Fig. 4, lower row. It is seen that at low photoelectron energy (i.e., near the center of the plot), the phase jumps by  $2\pi$  along the spiral curves, which resemble Coulomb spirals, shown in Fig. 3. The number of spiral arms is equal to the number of absorbed photons. The main difference between the phase momentum distributions in Figs. 4 and 3 is that the TDSE spirals are much more twisted. The reason for this feature is not clear. It could be caused by some inherent property of the TDSE solution procedure, which could give rise to a common  $p$ -dependent phase factor of the ionization amplitude. (We remark that such common

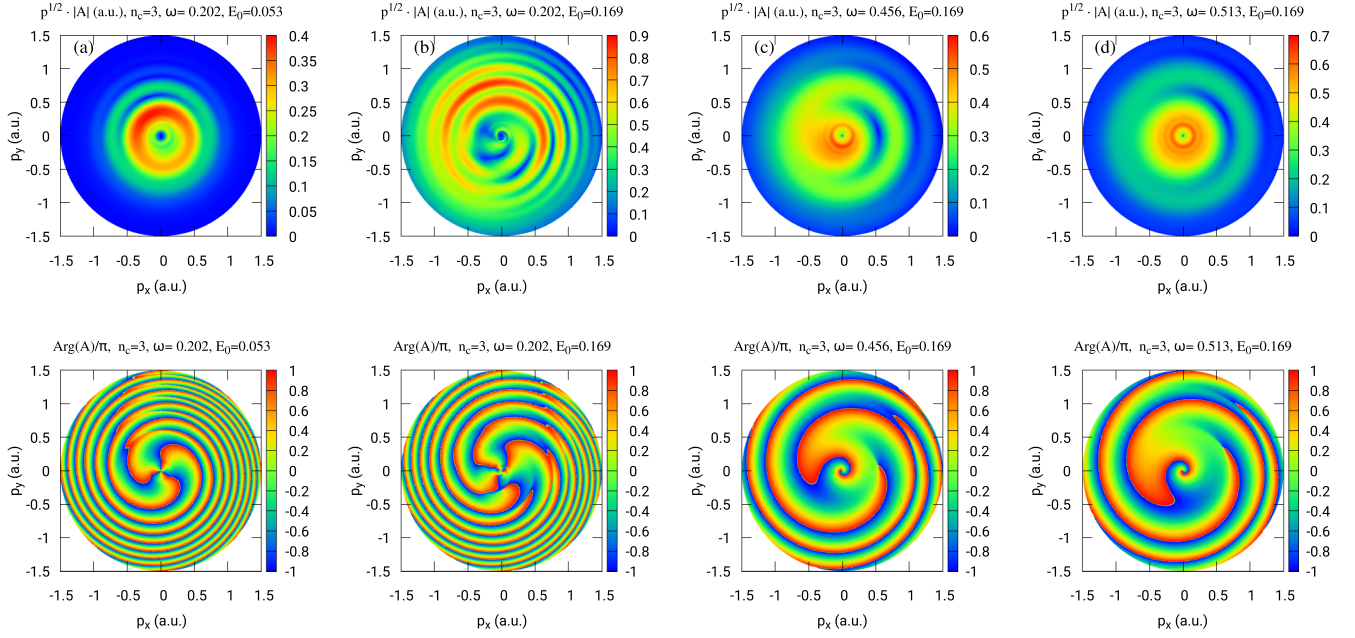


FIG. 4. Momentum distributions of the absolute values ( $\sqrt{p}|A|$ , upper row) and phase maps ( $\arg A$ , lower row) of the ionization amplitude for the initial 1-S ground state of the hydrogen atom for different values of the carrier frequency  $\omega$  and two intensities of the RCP pulse:  $10^{14}$  and  $10^{15}$  W/cm<sup>2</sup> (0.0534 and 0.1688 a.u., respectively).

phase factors do not affect the ionization probability.) For peak pulse fields  $\gtrsim 0.15$  a.u. and  $\omega < 0.4$  a.u., the spiral phase curves become distorted, see Fig. 4(b). This means that the multiphoton regime of the ionization is less adequate for such intensities, and the ionization amplitude for low photoelectron energy is determined by several ( $\sim 5$ ) PT terms, see Fig. 5(b).

The dependence of the absolute values of different terms of the expansion (13) on the photoelectron's momentum  $p$  is

shown in the upper row of Fig. 5. TDSE results demonstrate that for RCP pulses the terms in (31) with  $m \leq 0$  are negligibly small for all pulse parameters considered, which is in agreement with PT predictions (see previous Sec. II). Further, it is seen that with an increase of the carrier frequency  $\omega$ , the magnitude of the ionization amplitude is determined by only two terms of the partial expansion (13), see Fig. 5(c). The maximal contribution stems from the terms with  $m$  being equal to the minimal number of photons needed to overcome

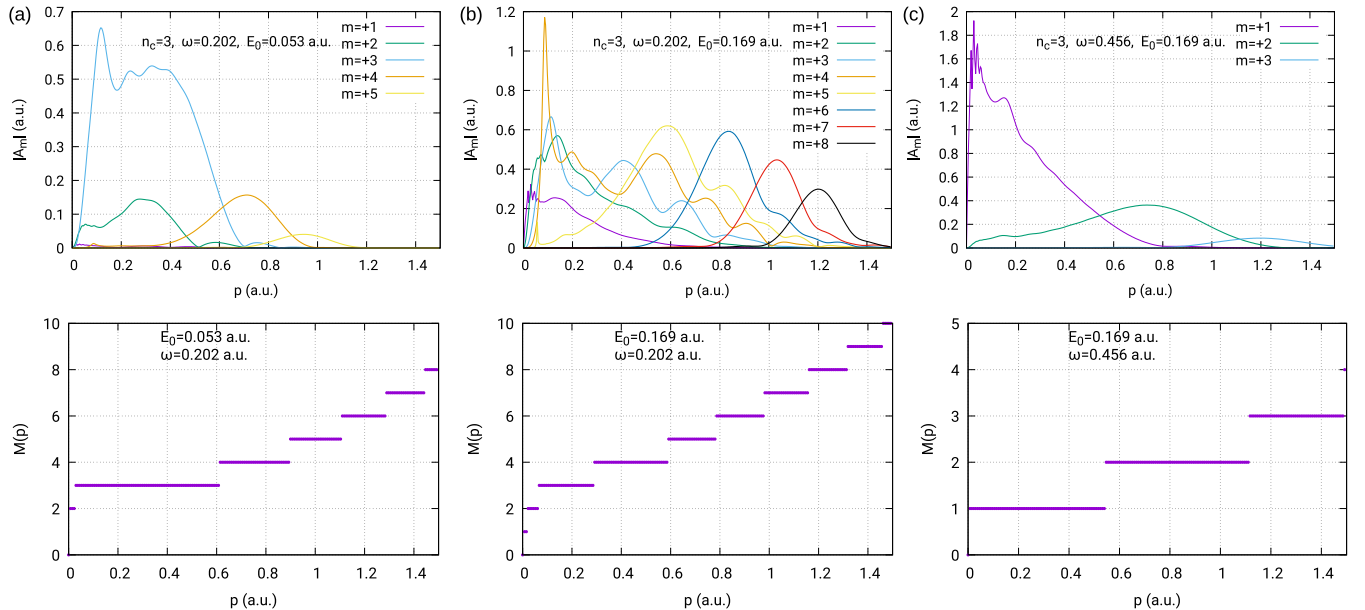


FIG. 5. Absolute values of the partial ionization amplitudes (upper row) vs total topological charge (lower row), enclosed by a circle with the radius  $p$ , for the ionization of the 1-S ground state of the hydrogen atom. The RCP pulse duration is three cycles of the carrier frequency  $\omega$  shown in corresponding panels. Peak pulse intensities are  $10^{14}$  W/cm<sup>2</sup> in the left column and  $10^{15}$  W/cm<sup>2</sup> otherwise.

the ionization threshold. The lower row in Fig. 5 shows the total topological charge inside a circle of the radius  $p$ . It is seen that with an increase of  $p$  the magnitude of the topological charge increases by unity. The similar behavior of the topological charge was also observed in the photodetachment process occurring in the strong-field regime [19].

Figures 5(a) and 5(c) demonstrate that jumps of the topological charge correspond to the crossings of the partial amplitudes, which is in agreement with the PT analysis of Sec. II B. For example, in Fig. 5(a) one observes that the curve of amplitude  $A_3$  crosses the curve for  $A_4$  close to the point  $p = 0.6$ . At this crossing the curve  $A_3$  goes down while  $A_4$  goes up. According to the PT treatment of Sec. II B, this means that there should be a vortex with the topological charge of  $+1$ . Indeed, this prediction is seen in the lower panel of Fig. 5(a), where the total topological charge inside the circle of the radius  $p \approx 0.6$  a.u. increases by  $+1$  from  $+3$  to  $+4$ . Simultaneously, in the phase map in Fig. 4(a), one can see the vortex near the point  $(-0.5, 0.3)$  in the  $xy$  plane. We emphasize that not every amplitude curve crossing causes a vortex formation. Namely, although the curves for  $A_2$  and  $A_4$  cross at  $p \approx 0.4$  a.u., there is no vortex seen on the phase map. This is because the total ionization amplitude in this point is dominated by a three-photon absorption amplitude  $A_3$  which is nonzero.

The situation becomes more complicated for high pulse intensities and lower pulse frequencies, see Fig. 5(b). Now the total ionization amplitude includes many partial amplitudes, corresponding to different numbers of absorbed photons. Nevertheless, the total topological charge always increases by  $+1$ , similarly to the case of high pulse frequencies. Apart from that, we observe a remarkable property of the ionization amplitude vortices for the low-frequency case (i.e., in the strong-field regime). Namely, in Fig. 5(b) one sees that starting from the fifth vortex, the locations of the vortices occur near the maximum of the corresponding partial amplitude. For example, the fifth vortex is located at  $p = 0.6$  a.u., where the radial amplitude  $A_{m=5}$  has maximum, the sixth vortex is located close to the maximum of the amplitude  $A_{m=6}$ , etc. Again, in all cases the increase in the total topological charge inside the circle as radius  $p$  increases from one vortex to another is equal to  $+1$ . Unlike the case when the total ionization amplitude is determined by two or three terms of the partial expansion, there is no simple explanation of this property of vortices emerging in the strong-field regime.

In Fig. 6 we present the momentum distribution of the absolute value and the phase of the ionization amplitude (left column) for the ionization of the 1-S ground state of the helium atom obtained by direct numerical solution of the corresponding six-dimensional TDSE [45]. The peak electric field of the two-cycle RCP pulse is  $E_0 = 0.2387$  a.u. (the corresponding intensity is  $2 \times 10^{15}$  W/cm<sup>2</sup>), the carrier frequency is  $\omega = 1.103$  a.u. (30 eV,  $\lambda = 41.3$  nm), and zero CEP. It is seen that the momentum distribution of the absolute value of the ionization amplitude has a high degree of circular symmetry. This means there is a small overlap of partial amplitudes corresponding to different numbers of absorbed photons. In Fig. 6(b) we observe that the parameter  $A_{m=2}$  has a maximum corresponding to a two-photon absorption, while  $A_{m=3}$  is maximal when three photons are absorbed, which

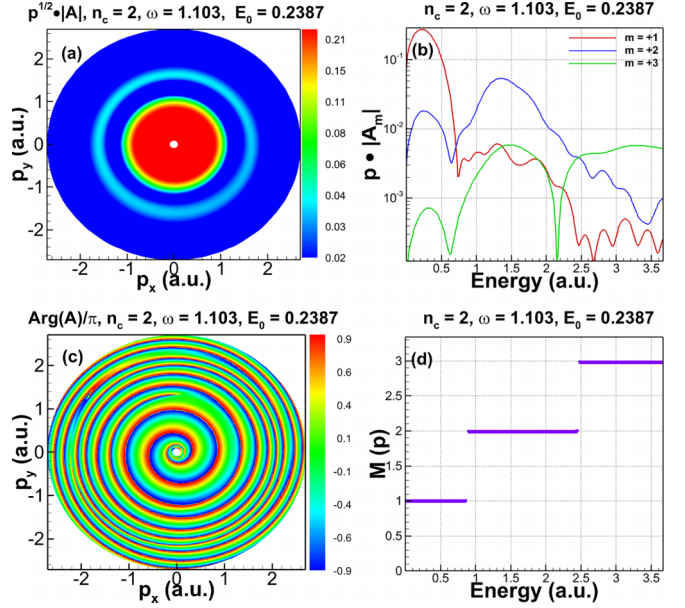


FIG. 6. TDSE numerical result for helium atom. Left column: The momentum distribution of the amplitude's absolute value,  $|A(\mathbf{p})|$  (a), and the phase  $\arg A(\mathbf{p})$ . (c) Right column: Logarithmic plot of the absolute values of the partial amplitudes (b) vs total topological charge (d) enclosed by the circle with the radius  $p$ . The two-cycle RCP pulse has peak intensity  $2 \times 10^{15}$  W/cm<sup>2</sup>, carrier frequency  $\omega = 1.103$  a.u. (30 eV), and zero CEP.

is in agreement with the PT description of the ionization process. The single arm Coulomb spiral in the phase map [Fig. 6(c)] means that the emission of the photoelectron with the momentum up to  $E \approx 0.5$  a.u. ( $p \approx 1.0$  a.u.) is caused by a single-photon absorption. It is also supported by the fact that the term  $A_1$ , describing the single-photon absorption, dominates in the total ionization amplitude up to  $E \approx 0.5$  a.u. ( $p \approx 1.0$  a.u.) [see Fig. 6(b)]. As  $p$  increases, Fig. 6(b) shows that  $A_1$  decreases while  $A_2$  increases and becomes comparable in magnitude, which leads to a quantum vortex at  $E = 0.8$  a.u. ( $p = 1.3$  a.u.), where the two amplitudes are equal. For  $E > 0.8$  a.u. ( $p > 1.3$  a.u.) the total amplitude is mostly determined by the two-photon absorption, i.e., by  $A_2$ . According to the PT treatment, the crossing of two dominating curves  $A_1$  and  $A_2$  should lead to the occurrence of a vortex with the topological charge  $+1$ . Indeed, by comparing the panels in the second column of Fig. 6, we have that the total topological charge increases by  $+1$  at the crossings of the amplitudes  $A_1, A_2$ , then  $A_2, A_3$  etc. These features of ionization amplitude vortices are completely analogous to those discovered in the ionization of the hydrogen atom, which means that the properties of the vortices described above should be the same for the ionization of any atomic target.

#### IV. CONCLUSION

In the present work we have considered the properties of the vortex states in the amplitude of atomic ionization by an intense few-cycle CP pulse. It was shown that the quantum vortices in the ionization amplitude for  $p > 0$  are determined by the interference of amplitude terms corresponding to the

absorption of different numbers of photons. When these numbers differ by unity (which was the case in numerical TDSE results), then the modulus of the topological charge of a vortex is also equal to unity. Positions of vortices in the momentum space are determined by both the absolute values of the interfering PT amplitudes and their relative phases. We emphasize that the general properties of the considered interference effects are not determined by features of a particular atom, but they are inherent to the very process of the ionization of finite quantum systems by short CP pulses, performed in the multiphoton regime. Therefore, results presented above should be taken into account when developing efficient methods of numerical analysis of the interaction of atoms and molecules with few-cycle CP pulses.

It is well known that phases of the ionization amplitude terms play a crucial role in the electron interference effects [40,50,61]. Above, we have found that spiral patterns emerge in the phase maps of the ionization amplitude for short CP pulses in the form of ‘‘Coulomb spirals’’ (see Sec. II C). Similar spiral patterns occur in the PMDs of the ionization probability in atoms and molecules [40–44] for electrons ionized by a pair of counter-rotating CP pulses. However, these two kinds of spirals are substantially different, both physically and mathematically. Physically, the Coulomb spirals are not seen in the PMDs of the ionization probability for atoms irradiated by an isolated CP pulse. They only occur in the *phase* maps of the ionization amplitude. Mathematically, the PMD spirals in the probability of the ionization by counter-rotating CP pulses are Fermat’s spirals, while Coulomb spirals are not; see Eqs. (28) and (30). Positions of quantum vortices in the ionization amplitude can be adjusted by firing the second CP pulse at an atom after a certain time delay  $\tau$ , similarly to the ionization scheme used in [40,45]. Then the magnitude of  $\tau$  as well as the intensity of the second (i.e., the probe) CP pulse can be used to control quantum vortices in momentum space. The corresponding analysis is the topic of forthcoming research. Another possibility to observe the predicted features of the momentum dependence of the ionization phase would be to consider the ionization by a few-cycle XUV pulse in the presence of an intense IR field. Such experiments are used to investigate the question of time delay in the photoionization [62]. The corresponding theoretical analysis, however, is complicated by the fact that terms in the multipole expansion (13) cannot be attributed to different PT orders with respect to the XUV pulse, since the presence of the IR field leads to the mixing of states with different angular momenta.

In our work we have not considered CEP effects. In the PT regime, when the ionization amplitude for a given  $p$  is determined by no more than three partial amplitude terms, the variation of CEP leads only to an overall rotation of the amplitude phase map, which is of no physical interest. Finally, we note that our PT analysis could be extended to the case of the ionization by elliptically polarized pulses, since they can be presented as a superposition of oppositely rotating CP pulses. The corresponding PT treatment, however, is complicated by the fact that the amplitude terms with the same dependence on the electron emission angle,  $\exp(im\varphi)$ , will be determined by several functions stemming from many PT orders and not by one or two terms, as in the case of CP pulses. This problem is the subject of further investigations.

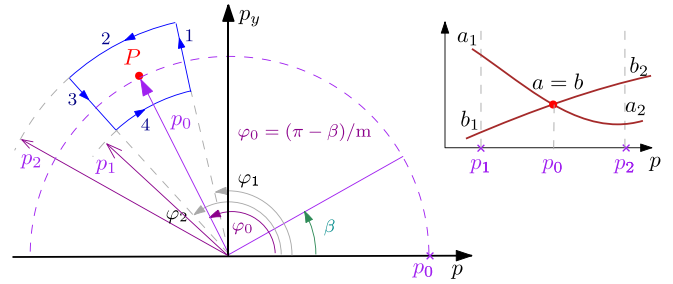


FIG. 7. The integration contour (blue lines on the left) enclosing the node point  $P$  with the polar coordinates  $(p_0, \varphi_0)$ , where  $\varphi_0 = (\pi - \beta)/m$  and  $a(p_0) = b(p_0)$ . On the right the crossing of amplitude curves are shown, which corresponds to the vortex with the topological charge  $+1$ .

## ACKNOWLEDGMENTS

The research of M.A.H.B.M.Y. and J.M.N.D. is supported by the US Department of Energy (DOE), Office of Science, Basic Energy Sciences (BES), under Award No. DE-SC0021054. Research of A.V.M. and N.L.M. is supported by the Ministry of Science and Higher Education of Russia through Project No. FZGU-2023-0007, and under Agreement No. 075-15-2021-1351 in part of the hydrogen atom ionization (N.L.M.). Computations were done using Stampede 2 at TACC under Grant No. PHY-120003. This work was completed utilizing Crane and Swan of the Holland Computing Center of the University of Nebraska, which receives support from the Nebraska Research Initiative.

## APPENDIX: CIRCULATION OF THE IONIZATION AMPLITUDE VELOCITY FIELD $a(p) + b(p) \exp i(\beta + m\varphi)$

Below we calculate the circulation of the velocity field (15) of the function  $A$  defined by

$$A(\mathbf{p}) = a(p) + b(p) e^{i(\beta + m\varphi)}, \quad (\text{A1})$$

where  $a$  and  $b$  are non-negative real-valued functions of the momentum  $p$ , and  $\beta$  is a real-valued function of  $p$ . We assume that  $A(\mathbf{p})$  has zero in the point  $P$  (see Fig. 7), whose polar coordinates are  $(p_0, \varphi_0)$ , where  $a(p_0) = b(p_0)$  and  $\varphi_0 = (\pi - \beta)/m$ .

The circulation (15) of the function (A1) over the contour, defined by Fig. 7, reduces to four integrals, two of which correspond to the radial segments, 1 and 3, and the other two correspond to the arc segments 2 and 4:

$$\Gamma(g) = \Gamma_1 + \Gamma_3 + \Gamma_2 + \Gamma_4. \quad (\text{A2})$$

The radial part of the circulation can be calculated as follows:

$$\begin{aligned} \Gamma_1 + \Gamma_3 &= \int_{p_1}^{p_2} \partial_p \ln(a + b e^{i(\beta + m\varphi_1)}) dp \\ &\quad - \int_{p_1}^{p_2} \partial_p \ln(a + b e^{i(\beta + m\varphi_2)}) dp \\ &= \ln \frac{a_2 + b_2 e^{i(\beta + m\varphi_1)}}{a_1 + b_1 e^{i(\beta + m\varphi_1)}} - \ln \frac{a_2 + b_2 e^{i(\beta + m\varphi_2)}}{a_1 + b_1 e^{i(\beta + m\varphi_2)}}, \quad (\text{A3}) \end{aligned}$$

where  $a_{1,2} = a(p_{1,2})$  and  $b_{1,2} = b(p_{1,2})$ . The angular part of the circulation (A2) is written

$$\Gamma_2 + \Gamma_4 = \int_{\varphi_1}^{\varphi_2} \partial_\varphi \ln(a_2 + b_2 e^{i(\beta+m\varphi)}) d\varphi - \int_{\varphi_1}^{\varphi_2} \partial_\varphi \ln(a_1 + b_1 e^{i(\beta+m\varphi)}) d\varphi. \quad (\text{A4})$$

The argument of the logarithm becomes a real negative number in the point  $\varphi_0$ ,  $\varphi_1 < \varphi_0 < \varphi_2$ , which is equal to either  $a_1 - b_1$  for  $a_1 < b_1$ , or  $a_2 - b_2$  for  $a_2 < b_2$  (the latter case is shown in Fig. 7). Either of the conditions must be met, since the functions  $a(p)$  and  $b(p)$  cross only once in the interval  $(p_1, p_2)$ , see Fig. 7. This implies that the integration contour encircles only *one* zero point  $P$ , see Fig. 7. Therefore we split integrals in Eq. (A4) in the point  $\varphi = \varphi_0$ . Accordingly, for the integral over path 2 of the contour we have

$$\begin{aligned} \Gamma_2 &= \int_{\varphi_1}^{\varphi_0} \partial_\varphi \ln(a_2 + b_2 e^{i(\beta+m\varphi)}) d\varphi \\ &+ \int_{\varphi_0}^{\varphi_2} \partial_\varphi \ln(a_2 + b_2 e^{i(\beta+m\varphi)}) d\varphi \\ &= \ln(a_2 - b_2 + i0) - \ln(a_2 + b_2 e^{i(\beta+m\varphi_1)}) \\ &+ \ln(a_2 + b_2 e^{i(\beta+m\varphi_2)}) - \ln(a_2 - b_2 - i0). \end{aligned} \quad (\text{A5})$$

We have to mention that the complex logarithm function is defined by  $\ln |z| e^{i \arg z} = \ln |z| + i \arg z$ , where  $-\pi \leq \arg z \leq \pi$ . Thus, for  $a_2 > b_2$  there is no problem, and the first and fourth terms in Eq. (A5) cancel out. Note that  $a_2 > b_2$  implies that  $a_1 < b_1$ , see Fig. 7. For  $a_2 < b_2$  (simultaneously  $a_1 > b_1$ ), the first term is  $i\pi + \ln |a_2 - b_2|$  and the fourth term is  $\ln(a_2 - b_2 - i0) = -i\pi + \ln |a_2 - b_2|$ . As a result, the integral  $\Gamma_2$

becomes

$$\Gamma_2 = \begin{cases} \tilde{\Gamma}_2, & \text{for } a_2 > b_2, (a_1 < b_1), \\ \tilde{\Gamma}_2 + 2\pi i, & \text{for } a_2 < b_2, (a_1 > b_1), \end{cases} \quad (\text{A6})$$

where

$$\tilde{\Gamma}_2 = \ln \left[ (a_2 + b_2 e^{i(\beta+m\varphi_2)}) / (a_2 + b_2 e^{i(\beta+m\varphi_1)}) \right]. \quad (\text{A7})$$

Similarly, for the integral  $\Gamma_4$ , we have

$$\Gamma_4 = \begin{cases} \tilde{\Gamma}_4, & \text{for } a_1 > b_1, (a_2 < b_2), \\ \tilde{\Gamma}_4 - 2\pi i, & \text{for } a_1 < b_1, (a_2 > b_2), \end{cases} \quad (\text{A8})$$

where

$$\tilde{\Gamma}_4 = \ln \left[ (a_1 + b_1 e^{i(\beta+m\varphi_1)}) / (a_1 + b_1 e^{i(\beta+m\varphi_2)}) \right]. \quad (\text{A9})$$

Noting the above Eqs. (A3)–(A9), the circulation Eq. (A2) becomes

$$\Gamma = \begin{cases} 2\pi i, & \text{for } a_1 > b_1, (a_2 < b_2), \\ -2\pi i, & \text{for } a_1 < b_1, (a_2 > b_2). \end{cases} \quad (\text{A10})$$

The consequence is that the topological charge of an isolated zero of the amplitude is equal to either +1 or -1. Moreover, for an amplitude having the form

$$A(\mathbf{p}) = a(p) + b(p) e^{i(\beta+m\varphi)}, \quad (\text{A11})$$

there are  $m$  vortices (each having unit strength with the same sign) for a single value of  $p = p_0$ , corresponding to the electron energy when both functions  $a$  and  $b$  coincide,  $a(p_0) = b(p_0)$ . These vortices are placed along a circle with the radius  $p_0$  in the emission  $xy$  plane, and the polar angles between the neighboring vortices are equal to  $(\beta - \pi)/m$ .

- 
- [1] K. Bliokh, I. Ivanov, G. Guzzinati, L. Clark, R. Van Boxem, A. B  ch  , R. Juchtmans, M. Alonso, P. Schattschneider, F. Nori, and J. Verbeeck, Theory and applications of free-electron vortex states, *Phys. Rep.* **690**, 1 (2017).
- [2] K. Y. Bliokh, Y. P. Bliokh, S. Savel'ev, and F. Nori, Semiclassical dynamics of electron wave packet states with phase vortices, *Phys. Rev. Lett.* **99**, 190404 (2007).
- [3] G. Thirunavukkarasu, M. Mousley, M. Babiker, and J. Yuan, Normal modes and mode transformation of pure electron vortex beams, *Philos. Trans. R. Soc. A* **375**, 20150438 (2017).
- [4] S. M. Lloyd, M. Babiker, G. Thirunavukkarasu, and J. Yuan, Electron vortices: Beams with orbital angular momentum, *Rev. Mod. Phys.* **89**, 035004 (2017).
- [5] A. S. Maxwell, G. S. J. Armstrong, M. F. Ciappina, E. Pisanty, Y. Kang, A. C. Brown, M. Lewenstein, and C. F. de Morisson Faria, Manipulating twisted electrons in strong-field ionization, *Faraday Discuss.* **228**, 394 (2021).
- [6] A. Surzhykov, D. Seipt, V. G. Serbo, and S. Fritzsche, Interaction of twisted light with many-electron atoms and ions, *Phys. Rev. A* **91**, 013403 (2015).
- [7] S. A.-L. Schulz, A. A. Peshkov, R. A. M  ller, R. Lange, N. Huntemann, C. Tamm, E. Peik, and A. Surzhykov, Generalized excitation of atomic multipole transitions by twisted light modes, *Phys. Rev. A* **102**, 012812 (2020).
- [8] V. P. Kosheleva, V. A. Zaytsev, R. A. M  ller, A. Surzhykov, and S. Fritzsche, Resonant two-photon ionization of atoms by twisted and plane-wave light, *Phys. Rev. A* **102**, 063115 (2020).
- [9] D. V. Karlovets, G. L. Kotkin, V. G. Serbo, and A. Surzhykov, Scattering of twisted electron wave packets by atoms in the Born approximation, *Phys. Rev. A* **95**, 032703 (2017).
- [10] V. Serbo, I. P. Ivanov, S. Fritzsche, D. Seipt, and A. Surzhykov, Scattering of twisted relativistic electrons by atoms, *Phys. Rev. A* **92**, 012705 (2015).
- [11] P. A. M. Dirac, Quantised singularities in the electromagnetic field, *Proc. R. Soc. A* **133**, 60 (1931).
- [12] J. O. Hirschfelder, A. C. Christoph, and W. E. Palke, Quantum mechanical streamlines. I. Square potential barrier, *J. Chem. Phys.* **61**, 5435 (1974).
- [13] J. O. Hirschfelder, C. J. Goebel, and L. W. Bruch, Quantized vortices around wavefunction nodes. II, *J. Chem. Phys.* **61**, 5456 (1974).
- [14] J. O. Hirschfelder, The angular momentum, creation, and significance of quantized vortices, *J. Chem. Phys.* **67**, 5477 (1977).
- [15] I. Bialynicki-Birula and Z. Bialynicka-Birula, Magnetic monopoles in the hydrodynamic formulation of quantum mechanics, *Phys. Rev. D* **3**, 2410 (1971).
- [16] I. Bialynicki-Birula, T. M  loduchowski, T. Rado  ycki, and C.   liwa, Vortex lines in motion, *Acta Phys. Pol. A* **100**, 29 (2001).

- [17] I. Bialynicki-Birula, Z. Bialynicka-Birula, and C. Śliwa, Motion of vortex lines in quantum mechanics, *Phys. Rev. A* **61**, 032110 (2000).
- [18] L. D. Landau and E. M. Lifshitz, *Quantum Mechanics* (Pergamon, New York, 1977).
- [19] F. Cajiao Vélez, Generation of quantum vortices in photodetachment: The role of the ground-state wave function, *Phys. Rev. A* **104**, 043116 (2021).
- [20] J. M. Rost, R. Gersbacher, K. Richter, J. S. Briggs, and D. Wintgen, The nodal structure of doubly-excited resonant states of helium, *J. Phys. B* **24**, 2455 (1991).
- [21] D. Bressanini and P. J. Reynolds, Unexpected symmetry in the nodal structure of the He atom, *Phys. Rev. Lett.* **95**, 110201 (2005).
- [22] T. C. Scott, A. Lüchow, D. Bressanini, and J. D. Morgan, Nodal surfaces of helium atom eigenfunctions, *Phys. Rev. A* **75**, 060101(R) (2007).
- [23] A. Lüchow and T. C. Scott, Nodal structure of Schrödinger wavefunction: General results and specific models, *J. Phys. B* **40**, 851 (2007).
- [24] J. M. Feagin, Vortex kinematics of a continuum electron pair, *J. Phys. B* **44**, 011001 (2010).
- [25] J. H. Macek, J. B. Sternberg, S. Y. Ovchinnikov, and J. S. Briggs, Theory of deep minima in  $(e, 2e)$  measurements of triply differential cross sections, *Phys. Rev. Lett.* **104**, 033201 (2010).
- [26] J. S. Briggs and J. M. Feagin, Scattering theory, multiparticle detection, and time, *Phys. Rev. A* **90**, 052712 (2014).
- [27] F. Navarrete and R. O. Barrachina, Vortices in the three-body electron–positron–proton continuum system induced by the positron-impact ionization of hydrogen, *J. Phys. B* **48**, 055201 (2015).
- [28] G. Petite, P. Agostini, and F. Yergeau, Intensity, pulse width, and polarization dependence of above-threshold-ionization electron spectra, *J. Opt. Soc. Am. B* **4**, 765 (1987).
- [29] H. G. Muller, H. B. van Linden van den Heuvell, P. Agostini, G. Petite, A. Antonetti, M. Franco, and A. Migus, Multiphoton ionization of xenon with 100-fs laser pulses, *Phys. Rev. Lett.* **60**, 565 (1988).
- [30] S. L. Chin, C. Rolland, P. B. Corkum, and P. Kelly, Multiphoton ionization of Xe and Kr with intense 0.62- $\mu\text{m}$  femtosecond pulses, *Phys. Rev. Lett.* **61**, 153 (1988).
- [31] W. Nicklich, H. Kumpfmüller, H. Walther, X. Tang, H. Xu, and P. Lambropoulos, Above-threshold ionization of cesium under femtosecond laser pulses: New substructure due to strongly coupled bound states, *Phys. Rev. Lett.* **69**, 3455 (1992).
- [32] W. M. Wood, C. W. Siders, and M. C. Downer, Measurement of femtosecond ionization dynamics of atmospheric density gases by spectral blueshifting, *Phys. Rev. Lett.* **67**, 3523 (1991).
- [33] M. Wollenhaupt, A. Assion, D. Liese, C. Sarpe-Tudoran, T. Baumert, S. Zamith, M. A. Bouchene, B. Girard, A. Flettner, U. Weichmann, and G. Gerber, Interferences of ultrashort free electron wave packets, *Phys. Rev. Lett.* **89**, 173001 (2002).
- [34] F. Cajiao Vélez, L. Geng, J. Z. Kamiński, L.-Y. Peng, and K. Krajewska, Vortex streets and honeycomb structures in photodetachment driven by linearly polarized few-cycle laser pulses, *Phys. Rev. A* **102**, 043102 (2020).
- [35] F. C. Vélez, K. Krajewska, and J. Z. Kamiński, Generation of electron vortex states in ionization by intense and short laser pulses, *Phys. Rev. A* **97**, 043421 (2018).
- [36] L. Geng, F. Cajiao Vélez, J. Z. Kamiński, L.-Y. Peng, and K. Krajewska, Structured photoelectron distributions in photodetachment induced by trains of laser pulses: Vortices versus spirals, *Phys. Rev. A* **104**, 033111 (2021).
- [37] L. Geng, F. Cajiao Vélez, J. Z. Kamiński, L.-Y. Peng, and K. Krajewska, Vortex structures in photodetachment by few-cycle circularly polarized pulses, *Phys. Rev. A* **102**, 043117 (2020).
- [38] O. I. Tolstikhin and T. Morishita, Strong-field ionization, rescattering, and target structure imaging with vortex electrons, *Phys. Rev. A* **99**, 063415 (2019).
- [39] Y. Kang, E. Pisanty, M. Ciappina, M. Lewenstein, C. F. de Morisson Faria, and A. S. Maxwell, Conservation laws for electron vortices in strong-field ionisation, *Eur. Phys. J. D* **75**, 199 (2021).
- [40] J. M. Ngoko Djiokap, S. X. Hu, L. B. Madsen, N. L. Manakov, A. V. Meremianin, and A. F. Starace, Electron vortices in photoionization by circularly polarized attosecond pulses, *Phys. Rev. Lett.* **115**, 113004 (2015).
- [41] J. M. Ngoko Djiokap, A. V. Meremianin, N. L. Manakov, S. X. Hu, L. B. Madsen, and A. F. Starace, Kinematical vortices in double photoionization of helium by attosecond pulses, *Phys. Rev. A* **96**, 013405 (2017).
- [42] J. M. Ngoko Djiokap, A. V. Meremianin, N. L. Manakov, L. B. Madsen, S. X. Hu, and A. F. Starace, Dynamical electron vortices in attosecond double photoionization of  $\text{H}_2$ , *Phys. Rev. A* **98**, 063407 (2018).
- [43] K.-J. Yuan, H. Lu, and A. D. Bandrauk, Photoionization of triatomic molecular ions  $\text{H}_3^+$  by intense bichromatic circularly polarized attosecond UV laser pulses, *J. Phys. B* **50**, 124004 (2017).
- [44] K.-J. Yuan, S. Chelkowski, and A. D. Bandrauk, Photoelectron momentum distributions of molecules in bichromatic circularly polarized attosecond UV laser fields, *Phys. Rev. A* **93**, 053425 (2016).
- [45] J. M. Ngoko Djiokap, A. V. Meremianin, N. L. Manakov, S. X. Hu, L. B. Madsen, and A. F. Starace, Multistart spiral electron vortices in ionization by circularly polarized UV pulses, *Phys. Rev. A* **94**, 013408 (2016).
- [46] Z. Wang, Q. Zhen, Y. Sun, J.-H. Chen, and X.-S. Liu, Investigation of vortex arms in electron vortices by counter-rotating elliptically polarized attosecond laser pulses, *Commun. Theor. Phys.* **74**, 015501 (2021).
- [47] D. Pengel, S. Kerbstadt, D. Johannmeyer, L. Englert, T. Bayer, and M. Wollenhaupt, Electron vortices in femtosecond multiphoton ionization, *Phys. Rev. Lett.* **118**, 053003 (2017).
- [48] I. Dana and V. E. Chernov, Vortex structure and characterization of quasiperiodic functions, *J. Phys. A* **35**, 10101 (2002).
- [49] E. A. Pronin, A. F. Starace, M. V. Frolov, and N. L. Manakov, Perturbation theory analysis of attosecond photoionization, *Phys. Rev. A* **80**, 063403 (2009).
- [50] J. M. Ngoko Djiokap, N. L. Manakov, A. V. Meremianin, S. X. Hu, L. B. Madsen, and A. F. Starace, Nonlinear dichroism in back-to-back double ionization of He by an intense elliptically polarized few-cycle extreme ultraviolet pulse, *Phys. Rev. Lett.* **113**, 223002 (2014).
- [51] P. V. Demekhin and L. S. Cederbaum, Dynamic interference of photoelectrons produced by high-frequency laser pulses, *Phys. Rev. Lett.* **108**, 253001 (2012).
- [52] A. D. Müller, E. Kutscher, A. N. Artemyev, L. S. Cederbaum, and P. V. Demekhin, Dynamic interference in the

- resonance-enhanced multiphoton ionization of hydrogen atoms by short and intense laser pulses, *Chem. Phys.* **509**, 145 (2018).
- [53] M. Baghery, U. Saalman, and J. M. Rost, Essential conditions for dynamic interference, *Phys. Rev. Lett.* **118**, 143202 (2017).
- [54] N. L. Manakov, S. I. Marmo, and A. V. Meremianin, A new technique in the theory of angular distributions in atomic processes: The angular distribution of photoelectrons in single and double photoionization, *J. Phys. B* **29**, 2711 (1996).
- [55] Y. Klimova, S. Marmo, and A. Meremianin, Angular distribution of electrons in multiphoton ionisation of polarised lithium atoms, *Phys. Lett. A* **377**, 1439 (2013).
- [56] D. A. Varshalovich, A. N. Moskalev, and V. K. Khersonskii, *Quantum Theory of Angular Momentum* (World Scientific, Singapore, 1988).
- [57] V. Mosert and D. Bauer, Photoelectron spectra with QPROP and t-SURFF, *Comput. Phys. Commun.* **207**, 452 (2016).
- [58] V. Tulsy and D. Bauer, QPROP with faster calculation of photoelectron spectra, *Comput. Phys. Commun.* **251**, 107098 (2020).
- [59] M. Han, J.-B. Ji, T. Balčiūnas, K. Ueda, and H. J. Wörner, Attosecond circular-dichroism chronoscopy of electron vortices, *Nat. Phys.* **19**, 230 (2022).
- [60] N. L. Manakov, M. V. Frolov, B. Borca, and A. F. Starace, Multiphoton detachment of a negative ion by an elliptically polarized, monochromatic laser field, *J. Phys. B* **36**, R49 (2003).
- [61] C. F. de Morisson Faria and A. S. Maxwell, It is all about phases: Ultrafast holographic photoelectron imaging, *Rep. Prog. Phys.* **83**, 034401 (2020).
- [62] R. Pazourek, S. Nagele, and J. Burgdörfer, Attosecond chronoscopy of photoemission, *Rev. Mod. Phys.* **87**, 765 (2015).